Registration of CT and Intraoperative 3-D Ultrasound Images of the Spine Using Evolutionary and Gradient-Based Methods

Susanne Winter, Bernhard Brendel, Ioannis Pechlivanis, Kirsten Schmieder, and Christian Igel, *Senior Member, IEEE*

***Abstract*—A system for the registration of computed tomography and 3-D intraoperative ultrasound images is presented. Three gradient-based methods and one evolutionary algorithm are compared with regard to their suitability to solve this image registration problem. The system has been developed for pedicle screw insertion during spinal surgery. With clinical preoperative and intraoperative data, it is demonstrated that precise registration is possible within a realistic range of initial misalignment. Significant differences can be observed between the optimization methods. The covariance matrix adaptation evolution strategy shows the best overall performance, only four of 12 000 registration trials with patient data failed to register correctly.**

***Index Terms*—Computed-aided surgery, covariance matrix adaptation, evolution strategy, gradient methods, image registration, medical image processing.**

I. Introduction

IMAGE-GUIDED navigation is used in many different medical fields, including neurosurgery, orthopedics, and traumatology. It provides the surgeon with real-time visualization of his/her instruments placed in an image dataset (mostly preoperative computed tomography or magnetic resonance imaging). For this purpose, accurate registration of preoperative datasets within the coordinate system of the navigation system is crucial.

Multimodality registration means finding the coordinate transformation mapping between two image datasets from different imaging modalities. This requires the solution of a difficult optimization problem. In this paper, we present a system for the registration of computed tomography and intraoperative ultrasound images that was developed for pedicle screw insertion during spinal surgery. We focus on the optimization problem posed by the registration and compare different algorithms for its solution.

Manuscript received July 5, 2006; revised March 16, 2007. This work was supported by the Bundesministerium für Bildung und Forschung (Az.13N8079) and in part by Siemens AG Medical Solutions, Erlangen. This work was an activity of the Kompetenzzentrum Medizintechnik Ruhr (KMR), Bochum, Germany.

S. Winter and C. Igel are with the Institut für Neuroinformatik, Ruhr-Universität Bochum, Bochum 44780, Germany (e-mail: Susanne.Winter@neuroinformatik.rub.de).

B. Brendel is with Philips Research Laboratories Hamburg, 20099 Hamburg, Germany (e-mail: bernhard.brendel@philips.com).

I. Pechlivanis and K. Schmieder are with the Department of Neurosurgery, Ruhr-Universität Bochum, Bochum 44780, Germany (e-mail: Ioannis.Pechlivanis@rub.de; Kirsten.Schmieder@rub.de).

Digital Object Identifier 10.1109/TEVC.2007.907558

There exist many different methods for registration [1]–[5]. Most of the systems currently in use during navigation rely on landmark-based methods. Typically, the landmarks are anatomical structures or fiducial markers that are fixed to the skin surface. For registration, landmarks must be marked on the preoperative data, and during surgery they must be referenced with a pointing device. This procedure is time consuming, and the accuracy of the registration depends on the resolution of the preoperative dataset, the accuracy of the manual localization, the type of the marker, the relative movement, and the spatial distribution of the landmarks. To overcome these disadvantages many approaches use intraoperative imaging. Intraoperative image data are acquired, usually with a lower quality than the preoperative data. A navigation system is able to localize the position of the data in the operating room and also the position of the instruments. To integrate the more precise preoperative data with additional planning information, the two imaging modalities are registered. Since 2-D or 3-D intraoperative image data provide much more information than single landmarks, a higher accuracy can be achieved compared with the systems based on anatomical landmarks or skin markers (e.g., [6] and [7]).

Currently, implemented systems acquire intraoperative computed tomography (CT) or magnetic resonance imaging (MRI) data (e.g., [8]) and use the complete volume information [9] or segmented surfaces [10] for the registration of preoperative and intraoperative datasets. These methods lead to high accuracy in registration, but the disadvantages are the high costs of the intraoperative imaging systems, difficult intraoperative application, and additional radiation exposure in the case of CT.

In light of these drawbacks, diagnostic ultrasound constitutes an ideal intraoperative imaging modality. The images can be acquired swiftly and easily, the patient and the surgeon are not exposed to ionizing radiation, and the systems are much cheaper than CT or MRI. The major disadvantage of ultrasound, however, is its low imaging quality, especially with regard to bone structures of the spine.

Multimodality registration comprising ultrasound datasets is a challenging task since the representation of the morphology of diagnostic ultrasound differs in a number of properties from other imaging modalities such as MRI or CT. Ultrasound images show speckle [11], an effect caused by the interference of small, randomly distributed subresolution scatterers. Speckle causes noise, reduces contrast, and decreases spatial resolution. At material interfaces with high acoustic impedance differences,

total and specular reflection of ultrasound waves occurs. Thus, no imaging is possible beyond the tissue-bone interfaces. The specular reflection leads to the effect that only those parts of the bone surface can be imaged that are nearly orthogonal to the direction of sound propagation. Existing approaches for the registration of bone structures in CT- and ultrasound datasets address long bones [12], the pelvis [13], [14], and the spine [15]–[22]. As volume–volume registration methods are not feasible for the aforementioned reasons, all these approaches use surface–surface registration methods, after segmentation of bone surfaces in ultrasound and CT images. The greatest difficulty in the data processing is posed by the surface segmentation in the ultrasound images.

Automatic registration of patient data with these methods has been possible only for the pelvis [14]. The other work has been done on bone models without surrounding tissue in a water bath. We have presented an approach for navigation during spine surgery which works on patient data as well as on phantom data [23]–[27].

Navigation in spinal surgery is difficult. The registration of fiducial markers on the skin surface leads to high registration errors for the vertebral bones because of their large relative movement. The use of fiducial markers, which are screwed directly into the bones to improve the registration result, increases the invasiveness. Nevertheless, there is a high interest in navigation of spinal surgery because the principal drawback of a number of well-established surgical methods is their high degree of invasiveness. This invasiveness is primarily determined by the necessity of preparation of anatomical structures to provide sufficient spatial orientation.

A central procedure in spinal surgery is the insertion of pedicle screws, and we decided on this method as a first application of our approach. Pedicle screw insertion for rigid fixation of neighboring vertebrae is a method that provides high stability of the spine for different indications [28], [29]. The necessity of precision requires ample preparation of anatomical structures. The placement of the screws is difficult and necessitates good 3-D orientation on the part of the surgeon. The entry point and the spatial orientation of the screw must be defined. In the lumbar vertebrae, the pedicles have a thickness of more than 8 mm, while the screws have a diameter of about 5 mm.

In conservative pedicle screw insertion, the surgeon relies purely on an X-ray device for 2-D imaging and his/her own direct vision. Serious complications such as neurological or vascular damage can result from screw misplacement [30]. In addition, correct placement of the screw is necessary for long-term stability of the spine [31]. For this reason, different computer-assisted techniques [32] have been proposed to support the intraoperative procedure. The use of intraoperative image-guided navigation leads to good results with regard to the rate of correct inserted screws [33].

In this paper, we consider automatic registration of ultrasound and CT datasets of spinal bone structures. Section II introduces gradient-based and evolutionary algorithms (EAs) for solving the registration optimization problem with an emphasis on the two special methods we use. In Section III, we describe our system and algorithm for bone structure registration in CT and ultrasound images. The experiments are described in Section IV and discussed in Section V before the conclusion.

II. Optimization Methods

Many rigid registration algorithms require the solution of an optimization problem, namely, finding the best parameters of a coordinate transformation mapping between the two image datasets. The objective function is discontinuous, because of the finite resolution of the images, and has, in general, multiple (local) optima. Various methods to tackle this optimization problem have been proposed [2]. In this study, we consider two distinct classes of optimization algorithms: gradient-based approaches based on numerically estimated gradients, and evolutionary optimization.

In the following, we describe the optimization algorithms compared in our experiments with an emphasis on two special methods we use. As EAs are not as well-established as gradient methods, we briefly review their basic concepts and select previous applications of evolutionary computing to image registration in medicine.

In the following, let $f : \mathbb{R}^n \longrightarrow \mathbb{R}$ denote the objective function to be maximized. All methods are iterative algorithms, which successively modify solution vectors $\boldsymbol{x}^{(t)} = \left(x_1^{(t)}, \ldots, x_n^{(t)}\right) \in \mathbb{R}^n$, where n is the number of parameters to optimize and the superscript t indicates the iteration.

1) Gradient-Based Optimization: Gradient-based methods represent the state-of-the-art in optimizing cost functions for image registration. Here, we consider three different gradient-based approaches. We use two popular classical methods, the nonlinear conjugate gradient (CG) algorithm and a quasi-Newton method, the Broyden–Fletcher–Goldfarb–Shanno (BFGS) algorithm. Further, we apply the method of resilient backpropagation (Rprop), an optimization algorithm developed and frequently used in the context of neural network training.

2) Evolutionary Optimization: EAs are a class of iterative direct, randomized global optimization techniques based on principles of neo-Darwinian evolution theory. In canonical EAs, a set of individuals forming the parent population is maintained. Each individual has a genotype that encodes a candidate solution for the optimization problem at hand, here an n-dimensional, real-valued, object-variable vector. The fitness of an individual is equal to the objective function value at the point in the search space it represents. In each iteration of the algorithm, new individuals, the offspring, are generated by partially stochastic variations of parent individuals. The fitness of each offspring is computed and a selection mechanism that prefers individuals with better fitness chooses the new parent population from the current parents and the offspring. This loop of variation and selection is repeated until a termination criterion is met.

Optimization-based image registration is a discontinuous problem that may have many local optima because medical images are often noisy and may contain ambiguities. Since EAs are direct search methods that are, in general, less prone to

getting stuck in suboptimal local maxima than are greedy ascent methods, there has been interest in evolutionary optimization of registration problems since the beginnings of image registration [34], [35].

In general, approaches to medical image registration using EAs reported in the literature (e.g., [36]–[43]) have led to good results. In most comparative studies, they are superior to alternative methods in terms of registration rates. However, three disadvantage of EAs for registration have been identified by several authors. First, the final results may not be as exact as the results achieved by gradient-based methods, mostly because some EAs discretize the search space. Second, EAs are not among the fastest methods for image registration. Further, some EAs share the common drawback of many optimization algorithms: That manual adjustment of parameters of the optimization strategy itself, the so-called hyperparameters, is necessary.

In this study, we propose to use the CMA-ES, [44]–[47] for image registration. Evolution strategies (ES) [48] are one of the main branches of EAs and are particularly well suited for real-valued optimization. The highly efficient CMA-ES, which is described in detail in Section II-C, overcomes the disadvantages of traditional EAs listed above. In the following, we concisely describe the optimization algorithms considered in our study, starting with the gradient-based methods.

A. CG and BFGS Algorithms

Both the CG algorithm and the BFGS algorithm are iterative gradient-based methods. In each step they determine a search direction and perform a line search in this direction. The direction is computed based on stored information from previous line searches and the current gradient in such a way that the exact maximum of an n-dimensional unimodal quadratic function is obtained within n line searches. Detailed descriptions of the CG and BFGS algorithms are beyond our scope, we refer to [49]–[51]. We use the nonlinear CG variant with the Polak–Ribière update rule and reset the search direction to the current gradient whenever a search direction is computed that is not an ascent direction. An elaborated direct (zeroth order) line search, which performed best in [52] is applied in both CG and BFGS algorithms.

B. Resilient Backpropagation

The Rprop algorithms are iterative gradient-based optimization methods with adaptive individual step sizes [52]–[55]. They are frequently used for neural network training as they are very fast and accurate, very robust with respect to their internal (hyper) parameters, first-order methods (i.e., time and space complexity scales linearly with the number of parameters to be optimized), easy to implement, and not very sensitive to numerical problems. In particular, the Rprop algorithms consider only the signs of the partial derivatives of the function to be optimized and not their amount. Therefore, they are suitable for applications where the objective function is noisy or the gradient is numerically estimated—as in the case of image registration. The Rprop algorithms are rarely applied in image registration. Müller *et al.* used Rprop for multimodal registration of 2-D images in [56], and for 3-D–2-D registration

foreach x_i **do**
  if $\partial f(\boldsymbol{x}^{(t-1)})/\partial x_i^{(t-1)} \cdot \partial f(\boldsymbol{x}^{(t)})/\partial x_i^{(t)} > 0$ **then**
    $\Delta_i^{(t)} = \min\left(\Delta_i^{(t-1)} \cdot \eta^+, \Delta_{\max}\right)$
    $x_i^{(t+1)} = x_i^{(t)} + \operatorname{sign}\left(\partial f(\boldsymbol{x}^{(t)})/\partial x_i^{(t)}\right) \cdot \Delta_i^{(t)}$
  else if $\partial f(\boldsymbol{x}^{(t-1)})/\partial x_i^{(t-1)} \cdot \partial f(\boldsymbol{x}^{(t)})/\partial x_i^{(t)} < 0$ **then**
    $\Delta_i^{(t)} = \max\left(\Delta_i^{(t-1)} \cdot \eta^-, \Delta_{\min}\right)$
    if $f(\boldsymbol{x}^{(t)}) > f(\boldsymbol{x}^{(t-1)})$ **then** $x_i^{(t+1)} = x_i^{(t-1)}$
    $\partial f(\boldsymbol{x}^{(t)})/\partial x_i^{(t)} := 0$
  else
    $x_i^{(t+1)} = x_i^{(t)} + \operatorname{sign}\left(\partial f(\boldsymbol{x}^{(t)})/\partial x_i^{(t)}\right) \cdot \Delta_i^{(t)}$

Fig. 1. The iRprop^+ algorithm with improved weight backtracking.

in [57]. They found that Rprop performed superior to standard gradient-descent and CG optimization [56].

In each iteration t of Rprop, each objective parameter $x_i^{(t)}$ is increased or decreased depending on whether the sign of the partial derivative $\partial f(\boldsymbol{x}^{(t)})/\partial x_i^{(t)}$ of the objective function with respect to the parameter is positive or negative. The amount of the update is equal to the individual step size $\Delta_i^{(t)}$, that is, we have

$$x_i^{(t+1)} = x_i^{(t)} + \operatorname{sign}\left(\frac{\partial f(\boldsymbol{x}^{(t)})}{\partial x_i^{(t)}}\right) \cdot \Delta_i^{(t)}.$$

Prior to this update, the step size is adapted based on changes of sign of the partial derivative in consecutive iterations. If the partial derivative changes its sign, indicating that a local maximum has been overstepped, then the step size is multiplicatively decreased; otherwise, it is increased: if $\partial f(\boldsymbol{x}^{(t-1)})/\partial x_i^{(t-1)} \cdot \partial f(\boldsymbol{x}^{(t)})/\partial x_i^{(t)}$ is positive then $\Delta_i^{(t)} = \eta^+ \Delta_i^{(t-1)}$, if the expression is negative, then $\Delta_i^{(t)} = \eta^- \Delta_i^{(t-1)}$, where $\eta^+ > 1$ and $\eta^- \in]0, 1[$.

Some Rprop variants implement weight backtracking. That is they partially retract "unfavorable" previous steps. Whether a parameter change was "unfavorable" is decided by a heuristic. We use an improved version of the original algorithm called iRprop^+, which is described in pseudocode in Fig. 1. The difference from the original Rprop proposed in [53] is that the weight-backtracking heuristic considers both the evolution of the partial derivatives and the overall error. For a comparison of iRprop^+ with other Rprop variants and a detailed description of the algorithms, the reader is referred to [52].

C. The CMA Evolution Strategy

In the following, we present the CMA-ES with weighted recombination [44], [45], [47]. Each individual represents an n-dimensional, real-valued, object-variable vector. These variables are altered by two variation operators, intermediate recombination, and additive Gaussian mutation. The former corresponds to computing the weighted center of mass of the μ individuals in the parent population. Mutation is realized by adding a normally distributed random vector with zero mean. The complete covariance matrix of the Gaussian mutation distribution is adapted during evolution to improve the search strategy.

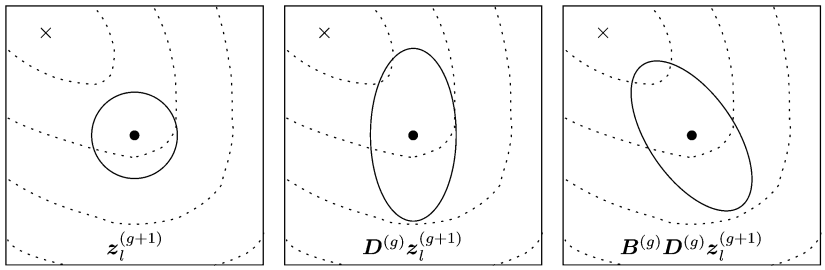

Fig. 2. The dashed lines schematically visualize an error/fitness surface (landscape) for a 2-D search space, where each line represents points of equal fitness and the × symbol marks the optimum. The dot corresponds to the center of mass of the parent population and the solid lines indicate the mutation ellipsoids (i.e., surfaces of equal probability density to place an offspring) of the random vectors after the different transformations. ES that adapt only one global step size can only produce mutation ellipsoids as shown in the left plot. Algorithms that adapt n different step sizes, one for each object variable, can produce mutation ellipsoids scaled along the coordinate axes like the one shown in the center plot. Only if the complete covariance matrix is adapted can arbitrary normal distributions be realized as shown in the picture on the right.

The CMA implements important concepts for strategy parameter adaptation. These allow for highly accurate adjustment of the search distribution, and therefore fast and accurate optimization, while requiring only small population sizes. The first concept is *derandomization*. That is, the mutation distribution is altered in a deterministic way such that the probability of reproducing steps in the search space that have led to the actual population is increased. Thereby the algorithm detects correlations between object variables and becomes invariant under orthogonal transformations of the search space (apart from the initialization). The second important concept is *cumulation*, which means using the information from previous generations efficiently by taking into account the search path of the population over a number of past generations.

The object parameters $\boldsymbol{x}_k^{(g+1)}$ of offspring $k = 1, \ldots, \lambda$ created in generation $g+1$ are given by

$$\boldsymbol{x}_k^{(g+1)} = \langle \boldsymbol{x} \rangle_{\boldsymbol{w}}^{(g)} + \sigma^{(g)} \boldsymbol{B}^{(g)} \boldsymbol{D}^{(g)} \boldsymbol{z}_k^{(g)}$$

where the $\boldsymbol{z}_k^{(g)} \sim \mathcal{N}(\boldsymbol{0}, \boldsymbol{I})$ are independent realizations of an n-dimensional normally distributed random vector with zero mean and covariance matrix equal to the identity matrix $\boldsymbol{I}$, $\sigma^{(g)}$ is the so-called global step size, and

$$\langle \boldsymbol{x} \rangle_{\boldsymbol{w}}^{(g)} = \sum_{i=1}^{\mu} w_i \boldsymbol{x}_{i:\lambda}^{(g)}$$

is the weighted mean of the selected individuals with $\sum_{i=1}^{\mu} w_i = 1$ and $w_i > 0$ for $i = 1, \ldots, \mu$. The index $i : \lambda$ denotes the ith best individual. We use superlinear weighted recombination and set $w_i := \ln(\mu + 1) - \ln i$. The covariance matrix $\boldsymbol{C}^{(g)}$ of the random vectors

$$\boldsymbol{B}^{(g)} \boldsymbol{D}^{(g)} \boldsymbol{z}_k^{(g)} \sim \mathcal{N}\left(\mathbf{o}, \boldsymbol{C}^{(g)}\right)$$

is a symmetric positive $n \times n$ matrix with

$$\boldsymbol{C}^{(g)} = \boldsymbol{B}^{(g)} \boldsymbol{D}^{(g)} \left(\boldsymbol{B}^{(g)} \boldsymbol{D}^{(g)}\right)^T.$$

The columns of the orthogonal $n \times n$ matrix $\boldsymbol{B}^{(g)}$ are the normalized eigenvectors of $\boldsymbol{C}^{(g)}$, and $\boldsymbol{D}^{(g)}$ is a $n \times n$ diagonal matrix with the square roots of the corresponding eigenvalues. Fig. 2 schematically shows the transformations of $\boldsymbol{z}_k^{(g)}$ by $\boldsymbol{B}^{(g)}$ and $\boldsymbol{D}^{(g)}$.

In the CMA-ES, rank-based (μ, λ)-selection is used. That is the μ best of the λ offspring form the next parent population. After selection, the strategy parameters, the matrix $\boldsymbol{C}^{(g)}$ and the global step size $\sigma^{(g)}$, are updated. For the covariance matrix, we have

$$\begin{aligned}
\boldsymbol{p}^{(g+1)} &= (1 - c_c) \cdot \boldsymbol{p}_c^{(g)} \\
&\quad + \sqrt{c_c(2 - c_c)} \frac{\sqrt{\mu_{\text{eff}}}}{\sigma^{(g)}} \left(\langle \boldsymbol{x} \rangle_{\boldsymbol{w}}^{g+1} - \langle \boldsymbol{x} \rangle_{\boldsymbol{w}}^{(g)} \right) \\
\boldsymbol{C}^{(g+1)} &= (1 - c_{\text{cov}}) \cdot \boldsymbol{C}^{(g)} + c_{\text{cov}} \cdot \boldsymbol{p}^{(g+1)} \left(\boldsymbol{p}^{(g+1)} \right)^T.
\end{aligned}$$

Herein, $\boldsymbol{p}^{(g+1)} \in \mathbb{R}^n$ is the evolution path—a weighted sum of the centers of the population over the generations starting from $\boldsymbol{p}^{(0)} = \boldsymbol{0}$ (the factor $\sqrt{\mu_{\text{eff}}}$ compensates for the loss of variance due to computing the center of mass). The parameter $c_c \in]0, 1]$ controls the time horizon of the adaptation of $\boldsymbol{p}$. The constant $\sqrt{c_c(2 - c_c)}$ normalizes the variance of $\boldsymbol{p}$ (viewed as a random variable) as $1^2 = (1 - c_c)^2 + \left(\sqrt{c_c(2 - c_c)}\right)^2$. The parameter $c_{\text{cov}} \in [0, 1[$ controls the update of $\boldsymbol{C}^{(g)}$. The influence of previous steps decays exponentially, where the decay rate is controlled by c_{cov}. The update rule for the covariance matrix shifts $\boldsymbol{C}^{(g)}$ towards the $n \times n$ matrix $\boldsymbol{p}^{(g+1)} \left(\boldsymbol{p}^{(g+1)}\right)^T$, which has rank 1, making mutation steps in the direction of $\boldsymbol{p}^{(g+1)}$ more likely.

The adaptation of the global step-size parameter σ is done separately on a shorter timescale (a single parameter can be estimated based on fewer samples than the complete covariance matrix). We keep track of a second evolution path $\boldsymbol{p}_\sigma$ without the scaling by $\boldsymbol{D}$

$$\begin{aligned}
\boldsymbol{p}_\sigma^{(g+1)} &= (1 - c_\sigma) \cdot \boldsymbol{p}_\sigma^{(g)} \\
&\quad + \sqrt{c_\sigma(2 - c_\sigma)} \cdot \boldsymbol{B}^{(g)} \boldsymbol{D}^{(g)^{-1}} \boldsymbol{B}^{(g)^T} \frac{\sqrt{\mu_{\text{eff}}}}{\sigma^{(g)}} \\
&\quad \cdot \left(\langle \boldsymbol{x} \rangle_{\boldsymbol{w}}^{(g+1)} - \langle \boldsymbol{x} \rangle_{\boldsymbol{w}}^{(g)} \right) \\
\sigma^{(g+1)} &= \sigma^{(g)} \cdot \exp\left(\frac{c_\sigma}{d_\sigma} \left(\frac{\|\boldsymbol{p}_\sigma^{(g+1)}\| - \hat{\boldsymbol{\chi}}_n}{\hat{\boldsymbol{\chi}}_n} \right) \right)
\end{aligned}$$

where χ_n is the expected length of a n-dimensional, normally distributed random vector with covariance matrix $\boldsymbol{I}$. It is approximated by $\sqrt{n}(1-(1/4n)+(1/21n^2))$. The damping parameter d_σ decouples the adaptation rate from the strength of the variation. The parameter $c_\sigma \in]0,1]$ controls the update of $\boldsymbol{p}_\sigma$.

If no selection occurred (i.e., if the new parents were selected from the offspring uniformly at random), the evolution path $\boldsymbol{p}_\sigma$ would be a weighted sum of independently normally distributed random variables starting form $\boldsymbol{p}_\sigma^{(0)} = \boldsymbol{0}$. Because of the normalization, its expected length would tend to $\hat{\boldsymbol{\chi}}_n$ for growing g. Hence, the update rule basically increases the global step size if the evolution path $\boldsymbol{p}_\sigma$ is larger than expected under uniform random selection and decreases the step size in the opposite case. If the path $\boldsymbol{p}_\sigma$ is shorter than $\hat{\boldsymbol{\chi}}_n$, then the steps that led to selected individuals cancelled each other out more strongly than expected (i.e., they tended to be anticorrelated) or the selected steps were smaller than expected. Thus, the step size σ should be decreased. Many successive steps in the same direction, which do not cancel out in $\boldsymbol{p}_\sigma$ and could have been realized by a single long step, lead to an evolution path $\boldsymbol{p}_\sigma$ that is larger than expected and the step size should be increased.

The parameters are set to the default values given in [47] (with $\mu_{\text{cov}} = 1$, i.e., we do not use the extension proposed in [46], because we use only small populations): $\lambda = 4 + \lfloor 3 \ln n \rfloor$, $\mu = \lfloor \lambda/2 \rfloor$, $c_\sigma = (10/n + 20)$, $d_\sigma = \max(1, (3\mu_{\text{eff}}/n + 10)) + c_\sigma$, $c_c = (4/4+n)$, and $c_{\text{cov}} = (2/(n+\sqrt{2})^2)$. In the initial population of the CMA-ES, all individuals are equal, that is all μ initial parents represent the same starting point. As the CMA-ES is a stochastic optimization method, it can be reasonable to consider κ independent CMA-ES populations starting from the same initial point in the search space. This strategy is called a $\kappa(\mu,\lambda)$-CMA-ES or in the following, for short, CMA_κ, where μ and λ become obvious from the problem dimension.

The CMA-ES addresses all the three potential problems observed when using EAs for medical image registration: limitations in accuracy and speed as well as difficulties in adjusting hyperparameters. The adaptation of the strategy parameters and the heuristics for the choice of hyperparameters (population sizes, etc.) of the algorithm make the CMA-ES a robust method, which does not require tuning for a specific problem class. As the CMA-ES adapts real-valued parameters, the accuracy of the evolved solutions does not suffer from discretization errors. This is in contrast to methods going back to [34]–[36] that are based on genetic algorithms using low-dimensional binary representations. The adaptation of the covariance matrix and the global step size lead to highly accurate optimization. By using the concepts of derandomization and cumulation, the CMA-ES efficiently exploits the information gathered in the evolutionary process. Therefore, small population sizes are sufficient. Together with the adapted strategy parameters this leads to very fast optimization. For a recent comparison of the CMA-ES with other EA, we refer to [58].

III. Bone Structure Registration of CT and Ultrasound Images

Our system integrates diagnostic ultrasound into navigated surgery. Fig. 3 gives an overview of the concept and the parts of the system. The CT data are acquired preoperatively and are used for conventional planning. These data are also preprocessed to extract the sampling points of the registration. Ultrasound images are acquired intraoperatively and preprocessed to enhance the bone surface imaging. The registration is done intraoperatively as well, and the result of the registration is transferred to the navigation system.

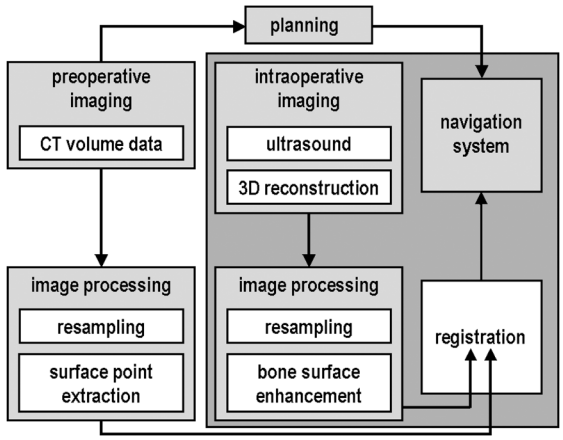

Fig. 3. Concept of the integration of ultrasound into navigated surgery on the spine.

In this study, we evaluate the precision of our registration on preoperatively obtained ultrasound data, as well as on intraoperatively acquired ultrasound data.

In the following, we first describe the steps of data processing as prerequisite of the registration which is described afterwards.

A. Three-Dimensional Ultrasound Data

Conventional ultrasound systems deliver 2-D images. To get a 3-D dataset, the position of the arbitrarily oriented ultrasound slices has to be determined. This can be achieved by using a magnetic or an optical tracking system. A magnetic system works with a sensor, fixed to the ultrasound transducer. This sensor identifies its movements in a predefined magnetic field. An optical tracking system consists of a stereo camera system that localizes well-defined reference bases. A reference base with infrared light-emitting diodes or infrared light-reflecting spheres is fixed to the transducer. Thus, the system can determine the position of the transducer. The relative position of the ultrasound image to the sensor or the reference base is determined by a unique calibration procedure.

During data acquisition, the transducer must be moved slowly and in such a way that the reference base is detectable for the system during the whole data acquisition. Excessively fast movement of the transducer results in data gaps in the reconstructed volume because the system can process only a limited number of images per time unit.

B. Data Preprocessing

The first step is resampling the datasets to obtain isotropic volume data. We use the MATLAB (The MathWorks, MA, USA) standard procedure resample to process the preoperative ultrasound data and vtkImageReslice of the vtk library [59] to resample the CT data. The voxel size is chosen as 0.5 mm $\times$ 0.5 mm $\times$ 0.5 mm. The intraoperative ultrasound data are reconstructed directly with this resolution.

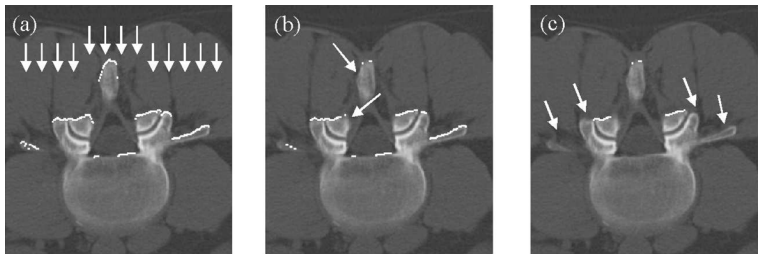

Fig. 4. (a) CT slice and all bone surface points that can be seen from dorsal, the arrows show the assumed direction of the sound propagation. (b) Estimation of the bone surface points that can be visualized by the ultrasound, the arrows mark the parts of the surface where the surface points were eliminated. (c) Surface after manual separation of one vertebra, the arrows mark the parts of the surface which belong to a neighboring vertebra.

1) Bone Surface Enhancement in Ultrasound: The ultrasound data are used as 3-D gray value datasets for registration and are preprocessed to enhance the bone surface structures. Since the brightness of ultrasound data is highly dependent on the examination and interferences of different tissue interfaces, first, the mean gray value of the axial slices is normalized.

Most ultrasound systems have implemented a processing step called depth gain compensation (DGC), where depth is meant with regard to the direction of sound propagation. The DGC has to be adjusted manually and is identical for all image lines. Assuming a linear transducer, the columns of an ultrasound image are identical with the image lines. An adaptive DGC (aDGC) is calculated depending on the content of an image line

$$\mathrm{aDGC}(\boldsymbol{p}) = \left(\sum_{y} u((p_1, y, p_3)) \right)^{q_{\mathrm{sum}}} \cdot u(\boldsymbol{p})^{q_{gv}}$$

where $u(\boldsymbol{p})$ describes the gray value at a point $\boldsymbol{p} = (p_1, p_2, p_3)$. The sum runs over all points in line with $\boldsymbol{p}$ in depth direction of the ultrasound image. The two parameters q_{sum} and q_{gv} allow weighting of the cumulative sum of the gray values and the gray values themselves. In our experiments, we used $q_{\mathrm{sum}} = 0.5$ and $q_{gv} = 2$

Considering the cumulative sum has the advantage that the result is a monotonic increasing function. A bright structure leads to a great increase of the aDGC, so that deeper structures are amplified more strongly. Since almost no sound propagates beyond a bone surface, this surface is the deepest bright structure and the aDGC will be nearly constant hereafter. Thus, the bone surface is amplified more than any overlying structure.

2) Surface Point Extraction From CT Data: The main step in the preprocessing of the CT data is the extraction of the surface points that are relevant for the registration. These are those bone surface points that lie on the target structure, the vertebra, and can also be detected by the ultrasound.

The visibility of bone surfaces in ultrasound images depends highly on the direction of the ultrasound propagation. Therefore, we simulate the sound propagation of ultrasound in the CT data. For the ultrasound data acquisition of the lumbar spine, we can presume that the transducer is moved from dorsal over the spinous processes. Thus, the imaging plane of the ultrasound correlates with an axial CT slice and the direction of the sound propagation correlates approximately to the posterior-anterior axis of the volume dataset. All bone surface points visible in the ultrasound images were extracted from the CT data by thresholding (200 Hounsfield units). Fig. 4(a) shows those parts of the bone surface hit by the virtual ultrasound. Additionally, we verified the angle between the surface and the sound propagation in order to include only parts of the surface that are nearly orthogonal to the sound propagation. Since we consider a linear array, the angle between the surface and the sound propagation is not calculated but roughly estimated. Only those surface points are selected that have more than two neighboring surface points with the same distance to the virtual ultrasound source [see Fig. 4(b)].

Due to the fact that adjacent vertebrae move relative to each other, it only makes sense to register single vertebrae. The surface points of different neighboring vertebrae were separated manually [Fig. 4(c)].

C. Objective Function and Stopping Criteria

Our approach, based on surface-volume registration, overcomes the abovementioned disadvantages of ultrasound bone registration by avoiding the segmentation of ultrasound data [23], [24].

We use a rigid surface-volume registration algorithm, where six transformation parameters, three for rotation and three for translation, have to be optimized. Since the tissue-bone interface is imaged as a bright area in the ultrasound data, the optimization criterion was chosen as the sum of the ultrasound gray values covered by the transformed surface points. Thus, the objective is to maximize the gray value sum, which can be written as follows:

$$\begin{aligned} &f(\alpha, \beta, \gamma, \Delta_x, \Delta_y, \Delta_z) \\ &\quad = f(\boldsymbol{x}) \\ &\quad = \sum_{i=1}^{N} u\Big(\boldsymbol{R}_{\alpha\beta\gamma} \cdot \boldsymbol{p}_i + (\Delta_x, \Delta_y, \Delta_z)^T \Big) \end{aligned}$$

where $\boldsymbol{R}_{\alpha\beta\gamma}$ is the rotation matrix that depends on the three angles α, β, and γ. The translational parameters Δ_x, Δ_y, and Δ_z are added after the rotation.

The gray value $u(x, y, z)$ at a distinct location is defined by trilinear interpolation, and we estimated the gradient in the parameter space (α, β, and γ in rad and x, y, z, Δ_x, Δ_y, and Δ_z in millimeters (mm)—in the following, we usually omit the units for convenience) by small steps of 10^{-9} in each direction.

In our experiments, we presume that we start the optimization after an initial preregistration at a configuration that is not too far from the optimum. In practice, we mark four points on the skin surface of the patient with a standard pointing device, as

well as in the CT data and preregister the images. In an intraoperative situation, it is realistic that we neither have to translate the images by more than ± 10 mm in each direction nor that the ultrasound device is twisted more than 0.2 rad in each coordinate. Thus, we optimize subject to box constraints to ensure that the optimization stays in this range. Without loss of generality, let us assume that we start with $(\alpha, \beta, \gamma, \Delta_x, \Delta_y, \Delta_z) = \mathbf{0}$. If a candidate solution is outside the region $[-0.2, 0.2]^3 \times [-10, 10]^3$ we call it infeasible and its objective function value is set to

$$f(\boldsymbol{x}) = \sum_{j=1}^{3} \min\{|x_j| - 0.2, 0\} + \sum_{i=4}^{6} \min\{|x_i| - 10, 0\}.$$

For optimization, we implemented the methods BFGS, CG, iRprop, and CMA-ES. The BFGS and CG algorithms were stopped if the progress of the line search in the search direction was zero. The iRprop algorithm was stopped if the step sizes of the rotation parameters were smaller than 0.002 rad and the step sizes of the translational parameters were smaller than 0.01 mm.

The CMA algorithm was stopped when

$$\frac{\max\left\{f\left(\boldsymbol{x}_{1:\lambda}^{(t')}|t'\right) = t, \ldots, t-k+1\right\}}{\min\left\{f\left(\boldsymbol{x}_{1:\lambda}^{(t')}|t'\right) = t, \ldots, t-k+1\right\}} - 1 \leq f_{\text{thr}}$$

that is, when the relative progress measured by monitoring the best individuals over the last k generations dropped below a predefined threshold. We set $f_{\text{thr}} = 10^{-6}$ and $k = 10$. This corresponds to an improvement in the fitness value of the last ten generations of 0.0001%.

In general, it is problematic to compare optimization algorithms with different stopping criteria. Thus, the experiments described below were additionally conducted with all algorithms using the same stopping criterion as the CMA, which is the only criterion of the three that is applicable to all four methods. However, it turned out that the three gradient-based methods performed much worse when the termination of the algorithm was determined by the relative progress as in the evolution strategy. Therefore, we only report results where each method uses its own stopping criterion as described above.

D. Multistart Optimization

We presume that the initial position is the result of a preregistration. Thus, the starting point already indicates a promising region of the search space. Nevertheless, as the objective function is usually multimodal, our algorithms may still get stuck in not globally optimal local maxima. Therefore, we consider multistart optimization. After the stopping criterion is met, the optimization algorithm can be restarted. The stochastic CMA-ES just starts again from the same initial position. All the strategy parameters of the CMA-ES are reset to their initial values. The large initial step sizes are sufficient for a different course of evolutionary optimization. The deterministic gradient-based methods have to be restarted from a different start position. The new starting point is determined by a random variation of the original initial position produced by the preregistration. This is done by adding the realization of a Gaussian random vector with zero mean and covariance matrix equal to $\boldsymbol{C}^{(0)}$ in the CMA-ES. That is, the restart of a gradient-based method can be viewed as a single initial mutation operation of the ES followed by the standard gradient-based optimization. We think that this allows a fair comparison of the optimization methods in a multistart scenario, in which the algorithms are finally stopped after a certain budget of objective function evaluations is exhausted.

IV. Experimental Evaluation

A. Data Acquisition

We took the preoperative and intraoperative ultrasound data of patients who underwent CT data acquisition of the lumbar spine for diagnostic purposes. The CT data were acquired in spiral technique with pixel sizes of about 0.3 mm $\times$ 0.3 mm. Slice thickness was 3 mm with a distance between the reconstructed slices of 1.5 mm.

The ultrasound data were acquired with a Siemens Sonoline Omnia system. The transducer we used was a 5 MHz curved array $(5.0C50+)$ for preoperative and a 3.5 MHz curved array (C5–2) for intraoperative application. Curved arrays provide an optimal coupling to the skin surface above the spinous processes of the lumbar spine. The broad field-of-view of these arrays allows images of the lamina, as well as of the transverse processes. The resolution of the two dimensional ultrasound images depends on the chosen image size and varied between 0.186 and 0.233 mm per pixel.

As the imaging quality is subject to strong individual variations the system parameters such as focus, imaging range, and DGC have to be chosen by visual judgment. A clear graphical representation of the lamina, the articular, and the transverse processes of the vertebrae is important.

Due to cost constraints, the preoperative data was acquired with a magnetic tracking system of 3-D Echotech. The intraoperative data were acquired with a considerably more accurate optical system. For this system, a precise calibration method that uses a simple spherical phantom was developed by our group [60]. For the intraoperative ultrasound data acquisition a reference base as described above was attached to one vertebra so that the reconstruction could be achieved by considering the movement caused by respiration.

The 3-D datasets were reconstructed by using the image data in combination with the position data [61]. The gray values of all ultrasound pixels are copied to the corresponding volume voxels. If there are different gray values projected to the same voxel they are averaged. We carried out the reconstruction without filling data gaps to avoid corruption of the data. The intraoperative data were directly preprocessed on the original 2-D ultrasound images by taking into account the real direction of the sound propagation. The cumulative sum was taken along the sound beam direction.

B. Patient Data

Our datasets used for registration comprise 12 vertebrae from five different patients. The preprocessing and the registered vertebrae are listed in Table I. The intraoperative dataset is denoted

TABLE I
ULTRASOUND DATASETS OF FIVE PATIENTS (P1–P5); DATA ACQUISITION PREOPERATIVE- (P) OR INTRAOPERATIVELY (I); PREPROCESSING WAS DONE ON VOLUME DATA SLICES (V) OR ON ORIGINAL ULTRASOUND SLICES (O); NUMBER OF TESTED LUMBAR VERTEBRAE

patient	acquisition	preprocessing	vertebrae
P1	p	v	L2, L3, L4
P2	p	v	L3, L4, L5
P3	p	v	L3, L4, L5
P4	p	v	L4, L5
P5	i	o	L5

by P5. All vertebrae were preregistered and the optimum was defined. No error occurred in the visual checking of the defined optimum.

C. Reference Registration

A ground truth registration can be determined only in phantom data. We showed in our phantom tests that the error between a point-based registration and our ultrasound registration was not more than 2 mm [27]. In these tests, the errors of the two methods are cumulative; thus, the error between the ultrasound registration and the ground truth is supposed to be less than this. For patient data, there exists no ground truth registration so a reference must be defined to assess the precision of the registration. Therefore, the optimum of the objective function that leads to the best match of the CT surface in the ultrasound data is determined. This match was defined for each vertebra in three steps: First, a rough manual registration was performed, followed by application of the registration algorithm 50 times within a small area. Finally, the plausibility of the result with the highest fitness value was visually checked. After definition of the reference registration for one vertebra, all subsequent surface positions are regarded relative to this reference registration.

To estimate the distance between a surface at a starting position and the defined optimum, or between a position after registration and the position in the defined optimum, the mean distance of all surface points $P = \{\boldsymbol{p}_1, \ldots, \boldsymbol{p}_N\}$ to their corresponding optimal positions $P^{\mathrm{opt}} = \{\boldsymbol{p}_1^{\mathrm{opt}}, \ldots, \boldsymbol{p}_N^{\mathrm{opt}}\}$ was defined as a distance measure

$$d(P, P^{\mathrm{opt}}) = \frac{1}{N} \cdot \sum_{i=1}^{N} \left\| \boldsymbol{p}_i^{\mathrm{opt}} - \boldsymbol{p}_i \right\|$$

where $\left\| \boldsymbol{p}_i^{\mathrm{opt}} - \boldsymbol{p}_i \right\|$ is the Euclidean distance between the point p_i and its optimal position p_i^{opt} and N is the number of surface points.

D. Evaluation

To evaluate the registration a set of 1000 starting positions was randomly generated by rotating and translating the reference solution. The set of starting positions consisted of points which are considered to be realistic misalignments in an intraoperative situation. The reference solution can be described by a translation vector $(\Delta_x, \Delta_y, \Delta_z)$ and three rotation parameters (α, β, γ). The data was generated by adding a displacement vector to the optimal values. The direction of this displacement vector was chosen uniformly at random. Its length was varied uniformly between 0 and 10 mm. The rotation parameters were varied similarly between 0 and 0.2 rad ($\approx 11.5°$).

Each vertebra was registered by the use of each of the four implemented optimization methods. The quality of the registration with the different optimization algorithms was assessed by the comparison of registration rate, computation time, and precision in finding the defined optimum. A registration trial was considered to be correct up to an average surface point distance of $d(P, P^{\mathrm{opt}}) \leq 1$ mm.

We considered two optimization scenarios. In the *single-trial* scenario, we started each algorithm from every starting point and stopped when the termination criterion was met. We analyzed the fraction of successful registrations, the number of objective function evaluations at feasible points, and the precision of the final result of these 1000 single trials per algorithm. In practice, it is more reasonable to assume that we have a predefined time window for the registration. Thus, we tested the algorithms in a *multistart* scenario with a limited budget of evaluations, as described in Section III-D. Each algorithm was stopped after 10 000 evaluations (in all about 5 s on a machine with $\mathrm{Intel}^{(\mathrm{R})}$ $\mathrm{Xeon}^{(\mathrm{TM})}$ 3.06 GHz CPU running Linux). The three gradient-based methods were allowed to finish their current iteration (e.g., the current line-search) and, therefore, stopped after slightly more than 10 000 evaluations. In both scenarios, in each trial, we keep track of the best solution found so far, which is returned as the final result.

The most time-consuming step of registration is the calculation of the objective function value, which is required for gradient estimation, line search, and fitness computation. Thus, the number of times the objective function value is calculated determines the computational complexity. Of course, the time needed to compute the objective function value for infeasible solutions can be neglected. Therefore, when we measure the computational complexity in evaluations we just count evaluations of feasible points.

V. RESULTS

A typical result of a registration of a preoperative dataset is presented in Fig. 5: In Fig. 5(a), an axial ultrasound slice is shown, Fig. 5(b) shows the bone surfaces of two vertebrae at the registered position of one of them, and Fig. 5(c) shows only the surface points of one of the two vertebrae. The corresponding CT slices are displayed underneath. Fig. 6 presents the registered intraoperative data: An ultrasound slice, the registered surface, and the corresponding CT are shown.

In all registration trials, we achieved solutions with the same or a worse quality than the reference registration.

The registration rates in the single trial scenario are given in Table II. The BFGS algorithm correctly registered 27.9%, the CG algorithm 55.1%, and the iRprop algorithm 64.4% of all trials. The CMA-ES registered 88.4% of the trials correctly. These differences in registration rates averaged over all vertebrae are highly significant (McNemar test, $p < 0.001$). The vertebra in the intraoperatively acquired data (P5L5) could be registered in 14.6% of the trials with BFGS, in 61.8% with CG,

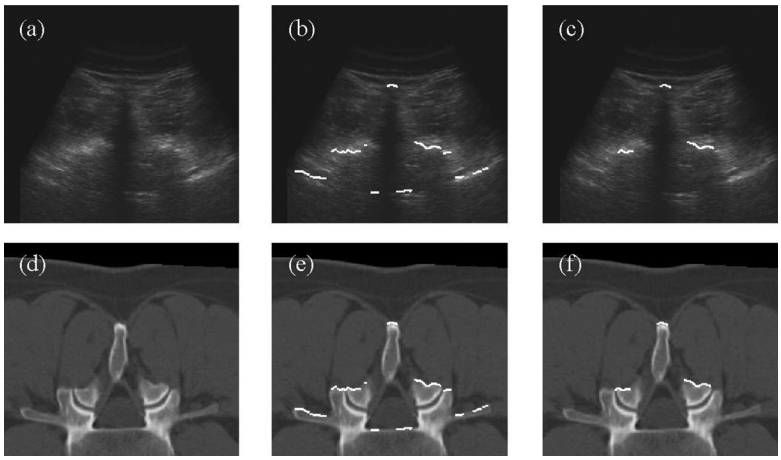

Fig. 5. (a) Preoperative axial ultrasound image. (b) Complete bone surface at the registered position of one vertebra. (c) Bone surface of one vertebra at the registered position. (d)–(f) Corresponding registered CT slices.

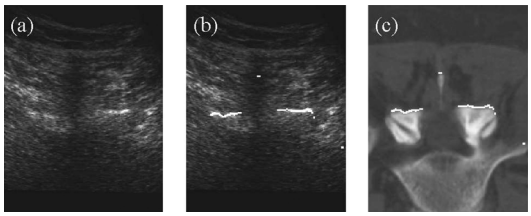

Fig. 6. (a) Intraoperative axial ultrasound image of a vertebra. (b) Bone surface at the registered position. (c) Corresponding CT image.

TABLE II
NUMBER OF CORRECT REGISTRATIONS IN THE SINGLE TRIAL OPTIMIZATION SCENARIO FOR 11 PATIENT VERTEBRAE, REGISTERED IN PREOPERATIVE DATA AND ONE VERTEBRA REGISTERED IN INTRAOPERATIVE DATA; EACH REGISTERED 1000 TIMES WITH DIFFERENT OPTIMIZATION METHODS, STARTING DISTANCES UP TO 11 MM. THE DIFFERENCES IN REGISTRATION RATES OVER ALL VERTEBRAE OF THE DIFFERENT OPTIMIZATION STRATEGIES ARE HIGHLY SIGNIFICANT (MCNEMAR TEST, $p < 0.001$)

single trial	BFGS	CG	iRprop	CMA-ES
P1L2	749	655	839	978
P1L3	552	497	575	806
P1L4	507	431	493	607
P2L3	365	653	786	910
P2L4	94	212	384	809
P2L5	134	651	779	948
P3L3	227	726	794	991
P3L4	140	534	529	883
P3L5	170	582	650	883
P4L4	153	604	664	931
P4L5	112	453	591	892
P5L5	146	618	643	970
P mean	279	551	644	884

and in 64.3% by the use of iRprop. The CMA-ES led to a registration rate of 97.0%.

Fig. 7 shows the cumulative distribution functions of the registration results in the single trial scenario for all 12 vertebrae. Each of the vertebrae was registered 1000 times with each of the four different optimization strategies. The plot shows the estimation of the probability that a trial reached a misalignment of less than a given distance. That is, for the fixed distance of 1 mm the results in the plot correspond to the mean number of correct

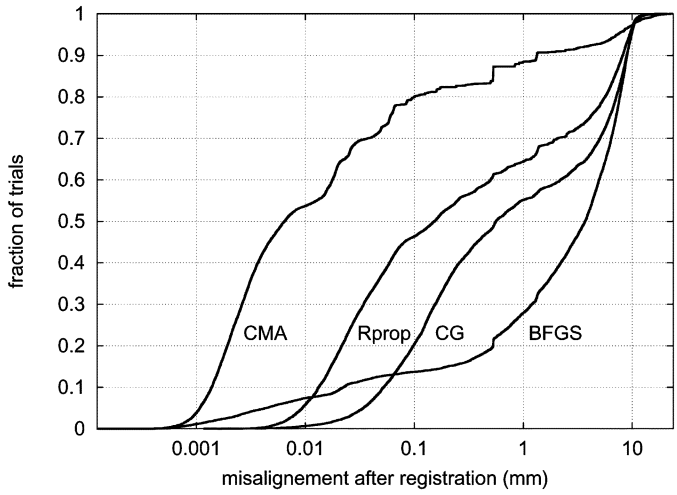

Fig. 7. Misalignment of all registration trials in the single trial optimization scenario; registration of 12 vertebrae, each with 1000 different starting positions and the different optimization methods BFGS, CG, iRprop, CMA. The ordinate shows the fraction of trials with a final misalignment less than the value on the abscissa (e.g., 80% of all CMA-ES trials stopped with an misalignment of less than 0.1 mm). The misalignment is plotted on logarithmic scale.

registrations given in Table II. The fraction of trials in which the final distance to the optimum was less than 0.01 mm was 7.39% for BFGS, 0.67% for CG, 5.79% for iRprop, and 53.69% for CMA-ES. The fraction of trials in which the final misalignment was less than 0.1 mm was 13.73% for BFGS, 20.32% for CG, 46.33% for iRprop, and 79.98% for CMA-ES.

The registration rate depends highly on the starting misalignment. Fig. 8 shows for each method the probability of a successful registration depending on the initial misalignment estimated from all 12 000 single trials registrations.

The four algorithms differ significantly in the average number of objective function evaluations performed until the stopping criterion is met. Table III shows the necessary number of evaluations to obtain a result with the different optimization strategies. All differences are statistically significant (paired Wilcoxon rank sum test, $p < 0.001$). The iRprop algorithm is the fastest, with an average number of 691.6 steps. With 916.9

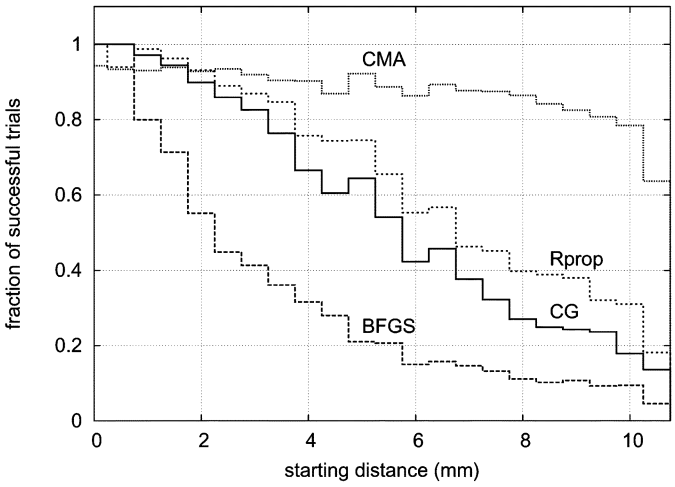

Fig. 8. Probability of successful registration depending on initial misalignment in the single trial optimization scenario.

TABLE III
MEAN, STANDARD DEVIATION (SD), MEDIAN, AND INTERQUARTILE RANGE (IQR) OF THE NUMBER OF OBJECTIVE FUNCTION EVALUATIONS OF ALL 12 000 REGISTRATION TRIALS FOR EACH OPTIMIZATION METHOD. ALL DIFFERENCES ARE STATISTICALLY SIGNIFICANT (PAIRED WILCOXON RANK SUM TEST, $p < 0.001$)

	BFGS	CG	iRprop	CMA-ES
mean	1145.8	7118.9	691.6	916.9
sd	885.9	6218.0	339.9	219.7
median	950	6346.5	648	900
iqr	1029.3	9410.8	396	187.5

steps on average, the CMA-ES is slightly faster than the BFGS with 1145.8 steps. The average number of steps needed by the CG is very large, 7118.9 steps. The CG results have larger standard deviation (and interquartile range).

In the multistart, the BFGS algorithm registered 47.3%, the CG algorithm 65.9%, and the iRprop 96.7% of all trials. The CMA-ES was able to register 99.97%. The differences are highly significant (McNemar test, $p < 0.001$). The results for the intraoperative vertebra were 29.2%, 62.1%, 97.1%, and 100% for BFGS, CG, iRprop, and CMA-ES, respectively. The results for the multistart scenario for the different vertebrae are given in Table IV.

The cumulative distribution of the registration results in the multistart scenario is shown in Fig. 9. Of course, in all multistart trials, the final objective function values (not shown) are at least as good as in the corresponding single trials. The fraction of registrations in which the final distance to the optimum was less than 0.01 mm was 17.36% for BFGS, 0.53% for CG 27.26% for iRprop, and 95.4% for CMA-ES. The fraction of trials in which the final distance to the optimum was less than 0.1 mm was for 22.63% BFGS, 18.63% for CG, 88.29% for iRprop, and 99.85% for CMA-ES.

Fig. 10 shows for each method the probability of a successful registration depending on the initial misalignment estimated from the 12 000 multistart registrations.

TABLE IV
NUMBER OF CORRECT REGISTRATIONS IN THE MULTISTART OPTIMIZATION SCENARIO FOR 11 PATIENT VERTEBRAE, REGISTERED IN PREOPERATIVE DATA AND ONE VERTEBRA REGISTERED IN INTRAOPERATIVE DATA; EACH REGISTERED 1000 TIMES WITH DIFFERENT OPTIMIZATION METHODS, STARTING DISTANCES UP TO 10 MM. THE DIFFERENCES IN REGISTRATION RATES OVER ALL VERTEBRAE OF THE DIFFERENT OPTIMIZATION STRATEGIES ARE HIGHLY SIGNIFICANT (MCNEMAR TEST, $p < 0.001$)

multi-start	BFGS	CG	iRprop	CMA-ES
P1L2	990	900	1000	1000
P1L3	879	579	944	1000
P1L4	886	517	924	999
P2L3	703	928	1000	998
P2L4	141	267	895	1000
P2L5	255	799	994	1000
P3L3	496	827	997	1000
P3L4	280	577	941	999
P3L5	328	659	972	1000
P4L4	264	719	985	1000
P4L5	161	518	981	1000
P5L5	292	621	971	1000
P mean	473	659	967	1000

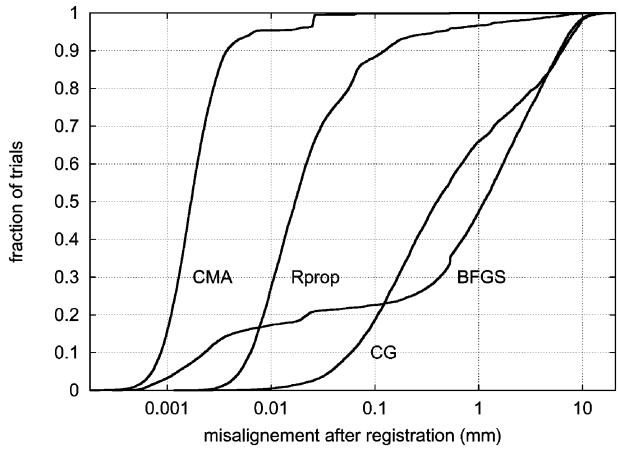

Fig. 9. Misalignment of all registration trials in the multistart optimization scenario; registration of 12 vertebrae, each with 1000 different starting positions and the different optimization methods BFGS, CG, iRprop, CMA.

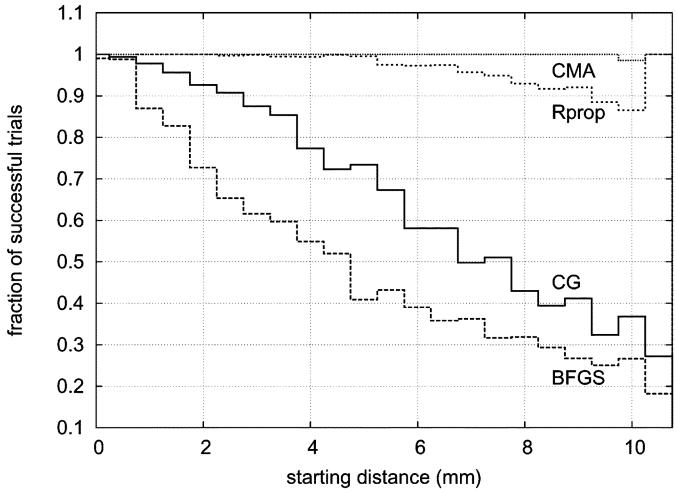

Fig. 10. Probability of successful registration depending on initial misalignment in the multistart optimization scenario.

VI. Discussion

The projections of the registered surfaces into the ultrasound data showed very good results in the preoperative data as well as in the intraoperative acquired ultrasound data.

In the single trial experiments, we observed big differences between the methods in terms of the registration rate and the precision. Here, the CMA-ES gave the best results. The CG and, in particular, the iRprop algorithms worked well for small starting distances. The BFGS algorithm seems to be not appropriate for our optimization problem. The methods differ also considerably in the number of objective function evaluations needed until the stopping criterion is met. The iRprop was the fastest algorithm, while giving reasonable registration rates for small initial misalignments (e.g., 98,7% for initial misalignments smaller than 1 mm, see Fig. 8). Thus, the use of the iRprop algorithm makes sense for a reregistration or real-time tracking of bone structures, where the initial misalignment is small but fast registration is important. The strong variability of the computation time needed by the CG can be interpreted as a sign of lacking robustness, see Table III. We regard this as a drawback of the CG method.

In the single-start trials, even the best method registered correctly in only 88.4% of all cases. Of course, a higher success rate is desirable during surgery. This can be achieved by the multistart strategy, which is also more appropriate in our application because, in practice, the registration algorithm has a predefined time window in which it has to produce a result. As the time until the stopping criterion is met differs between the four algorithms and there is often a tradeoff between speed and quality of the final solution, fixing the number of objective function evaluations per trial allows a better comparison of the optimization performance.

In the multistart experiments, all four methods showed increased registration rates. The multiple starts reduced the chance of getting stuck in a suboptimal local maximum of the multimodal objective function. However, the ranking of the methods in terms of the registration rate and the precision did not change when considering restarts. The CMA-ES showed excellent performance across all vertebrae and failed to register only four of 12 000 registration trials, see Table IV.

Not only the registration rate, but also the high precision of the CMA-ES is remarkable, see Figs. 7 and 9. In our experiments, the final misalignment is smaller compared with the results of the gradient-based methods. It is important to note that the better performance of the CMA-ES is obviously not due to a bias induced by the stopping criterion. The gradient-based methods performed much worse when the same termination criterion was used as in the evolution strategy.

There were considerable differences in the registration results among the vertebrae when using the gradient-based algorithms. Some of the vertebrae could be registered very well (e.g., P1L1), others rather badly, for example P2L4. The iRprop algorithm, the overall second best method in our comparison, showed a registration rate of less than 90% when applied to P2L4. These differences are due to the varying quality of the ultrasound data concerning the imaging of the bone structures. This quality depends on the ultrasound devices, on the patient as well as on the examiner. It is striking that in contrast to the gradient-based methods, the evolution strategy gave constantly good results across all vertebrae. This makes the CMA-ES the method of choice in our registration system.

VII. Conclusion

Diagnostic ultrasound is an ideal intraoperative imaging modality. The data can be acquired quickly and easily, the patient and the surgeon are not exposed to ionizing radiation, and the systems are much cheaper than CT or MRI. However, because of the limited quality of ultrasound images, it is necessary to compare the intraoperative image with precise preoperative data. Hence, an accurate algorithm for real-time multimodality registration is required.

We have presented a system for the registration of CT and intraoperative ultrasound images which was developed for pedicle screw insertion during spinal surgery. We have compared different optimization strategies with respect to their suitability to solve the registration problem, namely the gradient-based BFGS algorithm, conjugate gradient descent (CG), the improved resilient backpropagation algorithm (iRprop), and the covariance matrix adaptation evolution strategy (CMA-ES).

The CG and BFGS algorithms are well-known standard optimization methods. The iRprop is a robust gradient-based optimization algorithm originally developed for neural network training. The CMA-ES represents the state-of-the-art in real-valued evolutionary optimization. By means of an adaptation of the search distribution, the CMA-ES tackles the three potential problems that have been observed using EAs for medical image registration: limitations in accuracy and speed, and difficulties in adjusting hyperparameters.

We applied the four algorithms to the registration of CT datasets and 3-D ultrasound datasets of the spine. With our system, the registration turns out to be possible within an realistic intraoperative range of initial misalignment. This could be demonstrated with a number of clinical preoperative and intraoperative data.

Large performance differences have been observed between the optimization methods. The CMA-ES yielded the best results with regard to registration rate and precision. The iRprop algorithm outperformed the two established gradient-based methods, BFGS and CG, in terms of optimization speed, registration rate, and precision. The results of the comparison of Rprop and CG are in accordance with the findings reported in [56]. On a budget of 10 000 objective function evaluations, the CMA-ES registered correctly in almost 100% of our experiments. These 10 000 evaluations take only about 5 s in our current registration system. This allows convenient application during surgery.

It is likely that the individual results of the different algorithms can be further improved by tuning hyperparameters and also by applying a multiscale registration approach. However, in this study, we aimed to compare the different optimization algorithms in their canonical form with standard hyperparameter

settings to preclude a special adaptation to few datasets. Thus, we believe that the experimental findings can be extrapolated to other medical image registration problems.

We conclude that it is important to exercise care in choosing the optimization procedure for registration. We propose using the CMA-ES for general medical image registration tasks. If speed of registration is crucial and the initial misalignment is small, the iRprop algorithm provides an alternative, for example, for reregistration or real-time tracking of bone structure.

In our opinion, the good CMA-ES results in this study are not only interesting for the medical application, but also for evolutionary computation research in general, because fair comparisons between optimization methods based on numerically estimated gradients and evolutionary approaches are rare.

ACKNOWLEDGMENT

The authors thank N. Hansen for his valuable comments on the manuscript.

REFERENCES

[1] L. Brown, "A survey of image registration techniques," *ACM Comput. Surveys*, vol. 24, no. 4, pp. 325–376, 1992.

[2] J. B. A. Maintz and M. A. Viergever, "A survey of medical image registration," *Med. Image Anal.*, vol. 2, no. 1, pp. 1–36, 1998.

[3] C. R. Maurer and J. M. Fitzpatrick, "A review of medical image registration in interactive image guided neurosurgery," in *Amer. Assoc. Neurological Surgeons*, R. J. Maciunas, Ed., 1993, pp. 17–44.

[4] P. A. van den Elsen, E.-J. D. Pol, and M. A. Viergever, "Medical image matching—A review with classification," *IEEE Eng. Med. Biol.*, vol. 12, no. 1, pp. 26–39, 1993.

[5] B. Zitova and J. Flusser, "Image registration methods: A survey," *Image and Vision Comput.*, vol. 21, pp. 977–1000, 2003.

[6] F. Maes, A. Collignon, D. Vandermeulen, G. Marchal, and P. Suetens, "Multimodality image registration by maximization of mutual information," *IEEE Trans. Med. Imag.*, vol. 16, pp. 187–198, 1997.

[7] J. West, J. M. Fitzpatrick, M. Y. Wang, B. M. Dawant, C. R. Maurer, R. M. Kessler, R. J. Maciunas, C. Barillot, D. Lemoine, A. Collignon, F. Maes, P. Suetens, D. Vandermeulen, P. A. van den Elsen, S. Napel, T. S. Sumanaweera, B. Harkness, P. F. Hemler, D. L. G. Hill, D. J. Hawkes, C. Studholme, J. B. A. Maintz, M. A. Viergever, G. Malandain, X. Pennec, M. E. Noz, G. Q. Maguire, M. Pollack, C. A. Pellizzari, R. A. Robb, D. Hanson, and R. Woods, "Comparison and evaluation of retrospective intermodality brain image registration techniques," *J. Comput. Assisted Tomography*, vol. 21, pp. 554–566, 1997.

[8] D. Gering, A. Nabavi, R. Kikinis, N. Hata, L. J. O'Donell, W. E. L. Grimson, F. Jolesz, P. M. Black, and W. M. Wells, "An integrated visualization system for surgical planning and guidance using image fusion and open MR," *J. Magn. Reson. Imag.*, vol. 13, pp. 967–975, 2001.

[9] W. M. Wells, P. Viola, H. Atsumi, S. Nakajima, and R. Kikinis, "Multimodal volume registration by maximization of mutual information," *Med. Image Anal.*, vol. 1, no. 1, pp. 35–51, 1996.

[10] M. A. Audette, F. P. Ferrie, and T. M. Peters, "An algorithmic overview of surface registration techniques for medical imaging," *Med. Image Anal.*, vol. 3, pp. 201–17, 2000.

[11] B. A. J. Angelsen, *Ultrasound Imaging: Waves, Signals and Signal Processing*. Trondheim, Norway: Emantec AS, 2000.

[12] T. Ault and M. W. Siegel, "Frameless patient registration using ultrasonic imaging: A preliminary study," *J. Image Guided Surgery*, vol. 1, pp. 94–102, 1995.

[13] D. V. Amin, T. Kanade, A. M. DiGioia, III, and B. Jaramaz, "Ultrasound registration of bone surface for surgical navigation," *Comput. Aided Surgery*, vol. 8, no. 1, pp. 1–16, 2003.

[14] J. Tonetti, L. Carrat, S. Blendea, P. Merloz, J. Troccaz, S. Lavallee, and J. P. Chirossel, "Clinical results of percutaneous pelvic surgery. Computer assisted surgery using ultrasound compared to standard fluoroscopy," *Comput. Aided Surgery*, vol. 6, no. 4, pp. 204–211, 2001.

[15] J. L. Herring, B. M. Dawant, D. Muratore, C. R. Maurer, R. L. Galloway, and J. M. Fitzpatrick, "Surface-based registration of CT images to physical space for image-guided surgery of the spine: A sensitivity study," *IEEE Trans. Med. Imag.*, vol. 17, pp. 743–752, 1998.

[16] G. Ionescu, S. Lavallée, and J. Demongeot, "Automated registration of ultrasound with CT images: Application to computer assisted prostate radiotherapy and orthopedics," in *Proc. 2nd Int. Conf. Medical Image Comput. Comput.-Assisted Intervention (MICCAI)*., 1999, vol. 1679, Lecture Notes in Computer Science, pp. 768–777.

[17] J. Ioppolo, J. Kowal, and L.-P. Nolte, "Ultrasonic registration techniques," in *Proc. 2nd Annu. Meeting Int. Soc. Comput. Assisted Orthopaedic Surgery (CAOS)*, 2002, pp. 295–295.

[18] J. Kowal, C. A. Amstutz, and L.-P. Nolte, "On B-mode ultrasound based registration for computer assisted orthopaedic surgery," in *Proc. 1st Annu. Meeting Int. Soc. Comput. Assisted Orthopaedic Surgery (CAOS)*, 2001, pp. 35–35.

[19] D. M. Muratore, B. M. Dawant, and R. L. Galloway, "Vertebral surface extraction from ultrasound images for technology-guided therapy," in *Proc. SPIE*, 1999, vol. 3661, pp. 1499–510.

[20] D. M. Muratore, J. L. Herring, B. M. Dawant, and R. L. Galloway, "The effect of ultrasonic frequency transducer frequency on registration of ultrasound to CT vertebral images," in *Proc. SPIE*, 1999, vol. 3661, pp. 839–847.

[21] J. W. Trobaugh, P. J. Kessman, D. R. Dietz, and R. D. Bucholz, "Ultrasound in image fusion: A framework and applications," in *IEEE Ultrason., Ferroelect., Freq. Contr. Symp.*, 1997, pp. 1393–1396.

[22] P. K. Weber, J. C. Schlegel, J. Meiche, L. Peter, and U. Harland, "A system for ultrasound-based intraoperative navigation in spine-surgery," in *Proc. IEEE Ultrasound Symp.*, 2001, pp. 1361–4.

[23] B. Brendel, S. Winter, A. Rick, M. Stockheim, K. Schmieder, and H. Ermert, "Registration of 3D CT- and ultrasound-datasets of the spine using bone structures," *Comput. Aided Surgery*, vol. 7, pp. 146–155, 2002.

[24] S. Winter, B. Brendel, A. Rick, M. Stockheim, K. Schmieder, and H. Ermert, "Registration of bone surfaces, extracted from CT-datasets, with 3D-ultrasound," *Biomedizinische Technik*, vol. 47, no. 1, pp. 57–60, 2002.

[25] S. Winter, B. Brendel, and C. Igel, "Registrierung von Knochen in 3D-Ultraschall- und CT-Daten: Vergleich verschiedener optimierungsverfahren," in *Bildverarbeitung Für Die Medizin (BVM)*, H. Handels, J. Ehrhardt, A. Horsch, H.-P. Meinzer, and T. Tolxdorff, Eds., 2005, pp. 345–149.

[26] S. Winter, B. Brendel, and C. Igel, "Registration of bone structures in 3D ultrasound and CT data: Comparison of different optimization strategies," in *Comput. Assisted Radiology and Surgery (CARS)*, H. U. Lemke, K. Inamura, K. Doi, M. W. Vannier, and A. G. Farman, Eds. New York: Elsevier, 2005, vol. 1281, International Congress Series, pp. 242–247.

[27] B. Brendel, J. Siepermann, S. Winter, and H. Ermert, "In vivo evaluation and in vitro accuracy measurements for an ultrasound-CT registration algorithm," in *Comput. Assisted Radiology and Surgery (CARS)*, H. U. Lemke, K. Inamura, K. Doi, M. W. Vannier, and A. G. Farman, Eds., 2005, vol. 1281, International Congress Series, pp. 583–588.

[28] R. Roy-Camille, G. Saillant, and C. Mazel, "Internal fixation of the lumbar spine with pedicle screw plating," *Clinical Orthopaedics and Related Research*, vol. 203, pp. 7–17, 1986.

[29] A. D. Steffee, R. S. Biscup, and D. J. Sitowski, "Segmental spine plates with pedicle screw fixation—A new internal fixation device for disorders of the lumber and thoracolumbar spine," *Clinical Orthopaedics and Related Research*, vol. 203, pp. 45–53, 1986.

[30] T. Laine, K. Mäkitalo, D. Schlenzka, A. Tallroth, M. Poussa, and A. Alho, "Accuracy of pedicle screw insertion: A prospective CT study in 30 low back patients," *Eur. Spine J.*, vol. 6, no. 6, pp. 402–405, 1997.

[31] S. C. Acikbas, F. Y. Arslan, and M. R. Tuncer, "The effect of transpedicular screw misplacement on late spinal stability," *Acta Neurochirurgica*, vol. 145, no. 11, pp. 949–955, 2003.

[32] L. T. Khoo, S. Palmer, D. T. Laich, and R. G. Fessler, "Minimally invasive percutaneous posterior lumbar interbody fusion," *Neurosurgery*, vol. 51, no. 5, pp. 166–181, 2002.

[33] T. Laine, T. Lund, M. Ylikoski, J. Lohikoski, and D. Schlenzka, "Accuracy of pedicle screw insertion with and without computer assistance: A randomized controlled clinical study in 100 consecutive patients," *Eur. Spine J.*, vol. 9, no. 3, pp. 235–240, 2000.

[34] J. M. Fitzpatrick and J. J. Grefenstette, "Genetic algorithms in noisy environments," *Mach. Learn.*, vol. 3, pp. 101–120, 1988.

[35] V. R. Mandava, J. M. Fitzpatrick, and D. R. Pickens, III, "Adaptive search space scaling in digital image registration," *IEEE Trans. Med. Imag.*, vol. 8, pp. 251–262, 1989.

[36] D. L. G. Hill, D. J. Hawkes, N. A. Harrison, and C. F. Ruff, "A strategy for automated multimodality image registration incorporating anatomical knowledge and image characteristics," in *Process. Med. Imag.*, 1993, vol. 687, LNCS, pp. 182–196.

[37] C. Studholme, D. L. G. Hill, and D. J. Hawkes, "Automated 3D registration od MR and CT images of the head," *Med. Image Anal.*, vol. 1, no. 2, pp. 163–175, 1996.

[38] J.-M. Rouet, J.-J. Jacq, and C. Roux, "Genetic algorithms for a robust 3-D MR-CT registration," *IEEE Trans. Inf. Technol. Biomed.*, vol. 4, pp. 126–136, 2000.
[39] G. C. Kagadis, K. K. Delibasis, G. K. Matsopoulos, N. A. Mouravliansky, P. A. Asvestas, and G. C. Nikiforidis, "A comparative study of surface- and volume-based techniques for the automatic registration between CT and SPECT brain images," *Med. Phys.*, vol. 29, no. 2, pp. 201–213, 2002.
[40] M. Capek, L. Mroz, and R. Wegenkittl, "Robust and fast medical registration of 3D-multi-modality data sets," in *Proc. 9th Mediterranean Conf. Med. Biol. Eng., Comput., Medicon*, 2001, pp. 515–518.
[41] H. F. G. García, A. G. Vega, A. H. Aguirre, J. L. M. Zaleta, and C. A. C. Coello, *Robust multiscale affine 2D-image registration through evolution strategies*, ser. LNCS. Berlin, Germany: Springer-Verlag, vol. 2439, Parallel Problem Solving From Nature-PPSN VI, pp. 740–748.
[42] M. P. Wachowiak, R. Smolikova, Y. Zheng, J. M. Zurada, and A. S. Elmaghraby, "An approach to multimodal biomedical image registration utilizing particle swarm optimization," *IEEE Trans. Evol. Comput.*, vol. 8, pp. 289–301, 2004.
[43] L. Silva, O. R. P. Bellon, and K. L. Boyer, "Precision range image registration using a robust surface interpenetration measure and enhanced genetic algorithms," *IEEE Trans. Pattern Anal. Mach. Intell.*, vol. 27, no. 5, pp. 762–776, 2005.
[44] N. Hansen and A. Ostermeier, "Convergence properties of evolution strategies with the derandomized covariance matrix adaptation: The $(\mu/\mu, \lambda)$-CMA-ES," in *Proc. 5th Eur. Congr. Intell. Tech. Soft Comput. (EUFIT'97)*., Aachen, Germany, 1997, pp. 650–654.
[45] N. Hansen and A. Ostermeier, "Completely derandomized self-adaptation in evolution strategies," *Evol. Comput.*, vol. 9, no. 2, pp. 159–195, 2001.
[46] N. Hansen, S. D. Müller, and P. Koumoutsakos, "Reducing the time complexity of the derandomized evolution strategy with covariance matrix adaptation (CMA-ES)," *Evol. Comput.*, vol. 11, no. 1, pp. 1–18, 2003.
[47] N. Hansen and S. Kern, "Evaluating the CMA evolution strategy on multimodal test functions," in *Lecture Notes in Computer Science*, X. Yao, E. Burke, J. A. Lozano, J. Smith, J. J. Merelo-Guervós, J. A. Bullinaria, J. Rowe, P. Tiňo, A. Kabán, and H. P. Schwefel, Eds., 2004, vol. 3242, ser. LNCS, Proc. Parallel Problem Solving from Nature (PPSN VIII), pp. 282–291.
[48] H.-G. Beyer and H.-P. Schwefel, "Evolution strategies: A comprehensive introduction," *Natural Comput.*, vol. 1, no. 1, pp. 3–52, 2002.
[49] E. Polak, *Computational Methods in Optimization*. New York: Academic, 1971.
[50] W. H. Press, S. A. Teukolsky, W. T. Vetterling, and B. P. Flannery, *Numerical Recipes in C*, 2 ed. Cambridge, U.K.: Cambridge Univ. Press, 1994.
[51] J. R. Shewchuk, *An Introduction to the Conjugate Gradient Method Without the Agonizing Pain*, 1 1/4 ed. Pittsburgh, PA: School of Comput. Sci., Carnegie Mellon Univ., 1994.
[52] C. Igel and M. Hüsken, "Empirical evaluation of the improved Rprop learning algorithm," *Neurocomputing*, vol. 50, no. C, pp. 105–123, 2003.
[53] M. Riedmiller and H. Braun, "A direct adaptive method for faster backpropagation learning: The RPROP algorithm," in *Proc. IEEE Int. Conf. Neural Netw.*, E. H. Ruspini, Ed., 1993, pp. 586–591.
[54] M. Riedmiller, "Advanced supervised learning in multi-layer perceptrons—From backpropagation to adaptive learning algorithms," *Computer Standards and Interfaces*, vol. 16, no. 5, pp. 265–278, 1994.
[55] A. D. Anastasiadis, G. D. Magoulas, and M. N. Vrahatis, "New globally convergent training scheme based on the resilient propagation algorithm," *Neurocomputing*, vol. 64, no. C, pp. 253–270, 2005.
[56] U. Müller, J. Hesser, and R. Männer, "Fast rigid 2D-2D multimodal registration," in *Proc. 7th Int. Conf. Med. Image Comput. Comput.-Assisted Intervention (MICCAI 2004)*, C. Barillot, D. R. Haynor, and P. Hellier, Eds., 2004, vol. 3216, LNCS, pp. 887–894.
[57] U. Müller, S. Bruck, J. Hesser, and R. Männer, "Correction of C-arm projection matrices by 3D-2D rigid registration of ct-images using mutual information," in *Proc. 2nd Int. Workshop, Biomed. Image Registration, (WBIR 2003)*, J. C. Gee, J. B. A. Maintz, and M. W. Vannier, Eds., 2003, vol. 2717, LNCS, pp. 161–170.
[58] A. Auger and N. Hansen, "Performance evaluation of an advanced local search evolutionary algorithm," in *Proc. IEEE Congr. Evol. Comput. (CEC 2005)*., 2005.
[59] W. Schroeder, M. Martin, and B. Lorensen, *The Visualization Toolkit: An Object-Oriented Approach to 3D Graphics*, 2 ed. Englewood Cliffs, NJ: Prentice-Hall, 1998.
[60] B. Brendel, S. Winter, and H. Ermert, "A simple and accurate calibration method for 3D freehand ultrasound," *Biomedizinische Technik*, vol. 49, no. 2,2, pp. 872–873, 2004.
[61] R. San-Jose, M. Martin-Fernandez, P. P. Caballero-Martinez, C. Alberola-Lopez, and J. Ruiz-Alzola, "A theoretical framework to three-dimensional ultrasound reconstruction from irregularly-sample data," *Ultrasound in Med. Biol.*, vol. 29, no. 2, pp. 255–269, 2003.

Susanne Winter studied medicine at the University of Bochum, Bochum, Germany, and the University of Essen, Essen, Germany, and afterwards neuroinformatics at the University of Bochum.

She is working at the Institut für Neuroinformatik since 2001 and submitted her doctoral thesis recently. Main topics of her research are multimodal image registration, especially of 3-D ultrasound data, and classification of medical data.

Bernhard Brendel received the Diploma degree in electrical engineering from the RWTH Aachen University, Aachen, Germany, in 2000. After that, he started his Ph.D. dissertation project on the usage of ultrasound imaging for registration of bones in navigated surgery and received the Ph.D. degree from the University of Bochum, Bochum, Germany, in 2005.

Since 2006, he has been a Research Scientist at the Philips Research Laboratories, Hamburg, Germany, and works on simulation and reconstruction algorithms in diffuse optical tomography.

Ioannis Pechlivanis received his exam and the Doctoral degree in medicine from the Ruhr-University, Bochum, Germany.

He is member of the Faculty of Neurosurgery (resident) at the Knappschaftskrankenhaus University Hospital, Bochum. His research focuses on brain imaging techniques and ultrasound applications in neurosurgery.

Kirsten Schmieder studied medicine at the Heinrich-Heine University, Düsseldorf, Germany, and received her approbation in 1988 and earned the Doctoral degree from the Justus-Liebig University, Giessen, Germany, in 1992, and the Venia Legendi in neurosurgery at the Ruhr-University Bochum, Bochum, Grmany, in 2000.

She is currently Deputy Head of the Department of Neurosurgery at the Ruhr-University, Bochum, Germany. In 2006, she was appointment Associate Professor. She has headed various research groups focused on navigation, ultrasound, and robotics in neurosurgical applications

Christian Igel (M'02–SM'04) received the Diploma degree in computer science from the University of Dortmund, Dortmund, Germany, and the Doctoral degree from the Technical Faculty of the University of Bielefeld, Bielefeld, Germany.

He is Junior Professor of Optimization of Adaptive Systems at the Institut für Neuroinformatik and a faculty member of the International Graduate School of neuroscience, Ruhr-Universität Bochum, Bochum, Germany. His research focuses on machine learning and information processing in biological systems.